Density fluctuations in vibrated granular materials

Edmund R. Nowak, James B. Knight, Eli Ben-Naim, Heinrich M. Jaeger, and Sidney R. Nagel

The James Franck Institute and the Department of Physics, The University of Chicago, Chicago, Illinois 60637

We report systematic measurements of the density of a vibrated granular material as a function of time. Monodisperse spherical beads were confined to a cylindrical container and shaken vertically. Under vibrations, the density of the pile slowly reaches a final steady-state value about which the density fluctuates. We have investigated the frequency dependence and amplitude of these fluctuations as a function of vibration intensity Γ. The spectrum of density fluctuations around the steady state value provides a probe of the internal relaxation dynamics of the system and a link to recent thermodynamic theories for the settling of granular material. In particular, we propose a method to evaluate the compactivity of a powder, first put forth by Edwards and co-workers, that is the analog to temperature for a quasistatic powder. We also propose a stochastic model based on free volume considerations that captures the essential mechanism underlying the slow relaxation. We compare our experimental results with simulations of a one-dimensional model for random adsorption and desorption.

PACS: 81.05.Rm, 05.40.1j, 46.10.1z, 81.20.Ev

I. INTRODUCTION

One of the salient features of noncohesive granular materials is that they can be packed over a range of densities and still retain their resistance to shear. For example, a stable conglomeration of monodisperse spheres can exist with a packing fraction r ranging from $\rho \approx 0.55$ (the random loose packed limit) to $\rho \approx 0.64$ (the random close packed limit) and even to $\rho \approx 0.74$ (the crystalline state). Because thermal energies, $k_B T$, are insignificant when compared to the energy it takes to rearrange a single particle, each metastable configuration will persist indefinitely until an external vibration comes along to knock it into another state. Thus, no thermal averaging takes place to equilibrate the system. The density of the material is determined both by its initial preparation and by the manner in which it was handled or processed, since such activities normally introduce some vibrations into the material. The phase space for the granular medium is explored not by fluctuations induced by ordinary temperature but by fluctuations induced by external noise sources, such as vibrations. It is the goal of this paper to provide an experimental foundation for the use of such fluctuations as a probe of the dynamics as well as the microstructure of granular media in the quasistatic, densely packed limit.

Granular compaction involves the evolution from an initial low-density packing state to one with higher final density and provides a model system for nonthermal relaxation in a disordered medium. In a previous study [1], we focused on the approach to a final steady-state density as vibrations were applied to the system. In particular, we studied the density of monodisperse spherical particles in a tall cylindrical tube as a series of external excitations, consisting of discrete, vertical shakes or "taps, were applied to the container. Such data indicate that the compaction process is exceedingly slow: the density approaches its final steady-state value approximately logarithmically in the number of taps. A typical exam-

ple of such behavior, in Fig. 1, shows that in excess of 10^4 taps may be required before the density has relaxed to its steady-state value. However, if one vibrates for a long enough time a steady-state density, depending on the intensity of the taps, will be attained. Even after the density reaches the steady-state value, one can discern fluctuations in the density about that value: after each "tap, the density will be slightly higher or lower than it was before. These fluctuations are reminiscent of thermal fluctuations about an equilibrium state, yet such a connection so far has not been investigated experimentally.

In statistical mechanics the study of fluctuations is of great physical interest. The fluctuation-dissipation theorem relates the dissipative response of a system to an external perturbation with the microscopic dynamics of the system in a state of equilibrium. Energy fluctuations in thermal systems can be used to investigate the set of distinct, microscopic states that are accessible to a system maintained at a fixed temperature. Likewise, a study of density fluctuations in granular media may provide a framework for understanding the physical phenomenon of compaction, i.e., how a vibrated powder, that is not in a steady state, finally approaches a steady state.

In a granular system, density fluctuations from the steady state represent the different volume configurations accessible to particles subject to an external vibration. It is desirable to develop an analogy between the role that vibrations play in nonthermal systems, such as granular media, and the role of temperature in thermal systems. Theoretically, this issue was addressed by Edwards and co-workers [2-4] who introduced a statistical mechanics for powders. The idea is based on the assertion that an analogy can be drawn between the energy of a thermal system and the volume V occupied by a powder. The entropy S of a powder is defined in the usual sense, by the logarithm of the number of available configurations. Edwards and co-workers then put forth the concept of an effective temperature for a powder, called the compactiv-

ity X, which is defined as $X \equiv \partial V / \partial S$. The significance of this effective temperature is that it allows for the characterization of a static granular system. This is distinct from the case of rapid granular flows where a "granular temperature given by the mean-square value of the fluctuating component of the particle velocities can be written down [5-7]. The compactivity is then a measure of "fluffiness in the powder: when $X = 0$, the powder is in its most compact configuration, whereas for $X = \infty$ the powder is the least dense.

Recently, another approach [8-10] that describes the static packing of powders has adapted a statistical model that contains geometric frustration as an essential ingredient. For granular materials, frustration arises in the form of hard-core repulsive constraints and the interlocking of grains of different shapes, which prevents local rearrangements. Both the static and dynamic (in the presence of vibration and gravity) properties of this model exhibit complex behavior with features that are common to granular packing, such as the logarithmic relaxation of density under tapping [1].

In this paper, we make contact with these ideas through a detailed study of the process of granular compaction. In particular, we propose a method for evaluating the compactivity of a vibrated powder through a definition of a "granular specific heat and measurements of density fluctuations observed in the reversible regime of steady-state behavior. We also elaborate on a theoretical model [11,12], based on the idea that the rate of increase in volume density is exponentially reduced by the free volume, which captures many of the significant features of our experiments. A model addressing the compaction of binary mixtures consisting of grains with very different sizes was recently proposed by de Gennes [13]. That model is similar to ours in that it incorporates free volume constraints and also exhibits a similar inverse logarithmic dependence for the density relaxation.

In the next section we will describe the experimental de-tails of the system, review how to obtain reproducible and reversible densities, and present our results for the density fluctuations. In Sec. III we discuss several models in relation to our experimental results and motivate the relevance of free volume constraints for granular compaction. In Sec. IV, we present the theoretical model and the results of related simulations of compaction. Finally, in the last section we discuss the central result of this paper, namely, how our data can be related to thermodynamic approaches for understanding granular media.

II. EXPERIMENTAL RESULTS

Experimental method

The details of the experimental apparatus and measurement technique were published elsewhere [1]. Monodisperse, spherical soda-lime glass beads (of 2 mm diameter) were confined to a 1.88 cm diameter Pyrex tube measuring 1 m in height. The tube was subjected to discrete vertical shakes or taps! each consisting of one complete cycle of a 30 Hz sine wave. The vibration intensity was parametrized by Γ, which is the ratio of the peak acceleration A that occurs during a single tap to the gravitational acceleration $g = 9.8$ m/s^2: $\Gamma = A/g$. The beads were baked prior to loading in the tube and precautions were taken to minimize complications resulting from electrostatic charging, convection, and external humidity fluctuations. The column of beads was prepared in a low density initial state by flowing high pressure, dry nitrogen gas from the bottom to the top of the tube. The top layer of the beads was free to move, i.e., there was no load or dead-weight surcharge applied to the column of beads. The density, or equivalently the packing fraction ρ, which is the percentage of volume occupied by the beads, was determined either by a measurement of the total height of the beads within the tube or using capacitors that were mounted on the outside wall of the tube. For the latter, the capacitance was found to vary linearly with packing fraction. Each capacitor averaged the density over sections containing approximately 6000 beads. Measurements of ρ were taken as a function of time, i.e., number of taps t and as a function of the intensity of the vibrations, Γ. Corrections for instrumental drift were made by using simultaneously acquired data from a second, stationary tube (identically prepared with the same type of beads and connected to the same vacuum system). Our instrumentation allowed shaking intensities up to $\Gamma \approx 7$ and provided a resolution $\Delta \rho = 0.0006$ in measured packing fraction changes.

The desired outcome of a shake cycle is to provide clearly defined periods of uniform dilation of the bead assembly. During these periods of dilation the beads have some freedom to rearrange their positions relative to their neighbors and thereby replace one stable close-packed configuration by another. Previously [1,14], we have shown that the overall behavior of the compaction process is qualitatively similar at different depths into the container (see also Fig. (1). Spurious effects from continuous vibrations, such as period doubling or surface waves [12], were avoided by spacing the taps sufficiently far apart in time to allow the system to come to complete rest between taps. Also, by using a tall container with smooth, low-friction interior walls shear-induced dilation and granular convection were suppressed [15]. Although friction between beads and with the tube walls can affect the mechanical stability of a bead configuration, we argue below that the motion of beads is limited primarily by geometric constraints imposed by the presence of other beads, particularly at the high densities investigated here.

The ratio of the container diameter to the bead diameter can also influence the compaction process. For small values of this ratio, ordering (crystallization) induced by the container walls [16] will increase the measured packing fraction over its bulk value, leading to densities that

can exceed the random close-packed limit. This may be responsible for the high maximum packing fractions seen in Fig. (2). Previous studies [1,14] indicate that the qualitative behavior of the compaction process is similar for varying bead sizes. The container walls can also place constraints on the density fluctuations. Since it is our aim to investigate these density fluctuations, the choice of bead size was a compromise between maximizing the container-to-bead diameter ratio and not having the amplitude of the density fluctuations be obscured by statistical averaging over a large number of particles.
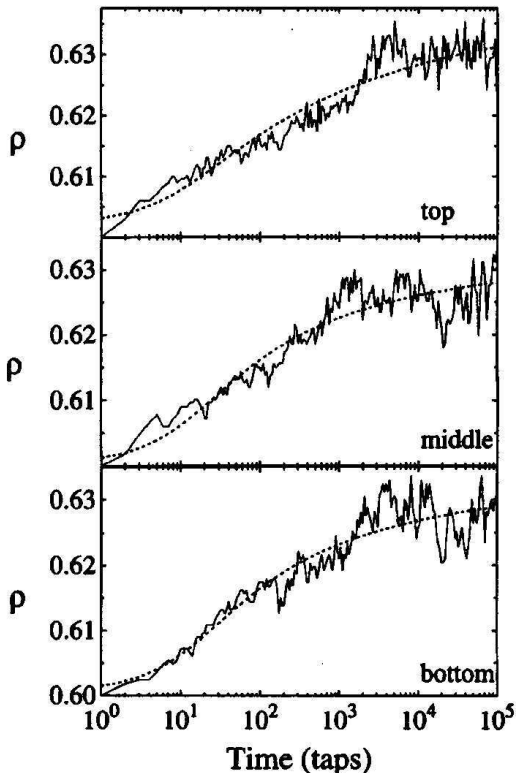
FIG. 1. The time evolution of the volume density ρ at three different depths near the top, middle, and bottom of the pile of beads. The curves represent a single run (no ensemble averaging! at a vibration intensity $\Gamma = 6.8$. The pile settles slowly from its initial low density configuration toward a higher steady-state density at long times, $t > 10^4$ taps. The dashed lines are fits to Eq. (1) with typical values of parameters: $0.637 < \rho_\infty < 0.647$, $0.036 < \Delta\rho_\infty < 0.044$, $0.20 < B < 0.40$, $10 < \tau < 18$.

Reaching the steady state

At a high acceleration Γ the steady-state density, ρ_{ss} can be approached by simply applying a very large number of taps (often greater than $10^4 - 10^5$). An example is shown in Fig. (1) for $\Gamma = 6.8$. The three panels correspond to the capacitively measured density near the top, middle, and bottom sections of the pile of beads. (The tap number t is offset by 1 tap so that the initial density can be included on the logarithmic axis.) Note that these curves represent a single run, and separate runs starting from the same initial density differ in the details of the density fluctuations but show a similar overall behavior. The behavior of $\rho(t)$, obtained by averaging many runs of this kind, appears to be homogeneous throughout the pile at these high accelerations. As discussed in Ref. [1], the time evolution of this ensemble averaged density is well fitted by the expression

$$\rho(t) = \rho_\infty - \frac{\Delta\rho_\infty}{1 + B\ln(1 + t/\tau)} \qquad (1)$$

where the parameters ρ_∞ , $\Delta\rho_\infty$, B, and τ depend only on the acceleration Γ. Equation (1) was found to fit the ensemble averaged density over the whole range $0 < \Gamma < 7$ better than other functional forms that were tried i.e., exponential, stretched exponential, or algebraic forms, see Ref. [1]. The dashed lines in Fig. (1) show a fit to Eq. (1). Here, the value of the final density, ρ , is approximately equal to the observed steady-state density ρ_{ss} .

For small values of Γ, however, ρ_∞ corresponds to a metastable state and not the steady-state density. In particular, for values of the applied acceleration $\Gamma < 3$, it is difficult, if not experimentally impossible, to reach the steady-state by merely applying a sufficiently large number of taps of identical intensity. In this case, the steady state can be reached by "annealing [14] the system. The annealing is controlled by the ramp rate, $\Delta\Gamma/\Delta t$, at which the vibration intensity is varied over time. Experimentally, we slowly raise the value of Γ from 0 to a value beyond Γ^* in increments of $\Delta\Gamma \approx 0.5$. At each intermediate value of Γ we apply $\Delta t = 10^5$ taps. Γ^* defines an "irreversibility point in the sense that, once it has been exceeded, subsequent increases as well as decreases in Γ at a sufficiently slow rate $\Delta\Gamma/\Delta t$ lead to reversible, steady-state behavior. We found that $\Gamma^* \approx 3$ for 1, 2, and 3 mm beads [14]. A typical run is shown in Fig. 2. Here we have used 2 mm beads, and started with an initial density of $\rho \approx 0.59$. The highest densities are achieved by annealing the system, i.e., decreasing Γ slowly from Γ^* back down to $\Gamma = 50$. If Γ is rapidly reduced to 0 (large $\Delta\Gamma/\Delta t$) then the system falls out of "equilibrium. This leads to lower final densities and a curve for $\rho(\Gamma)$ that is not reversible. A crucial result emerging from data such as in Fig. 2 is that along the reversible branch, the density is monotonically related to the acceleration. We note that in 3D simulations of granular compaction by Mehta and Barker [17] a similar monotonic decrease in steady-state volume fraction as a function of shaking intensity was found. Thus, only once the steady-state has been reached is there a single-valued correspondence between the average density and the applied acceleration.

3
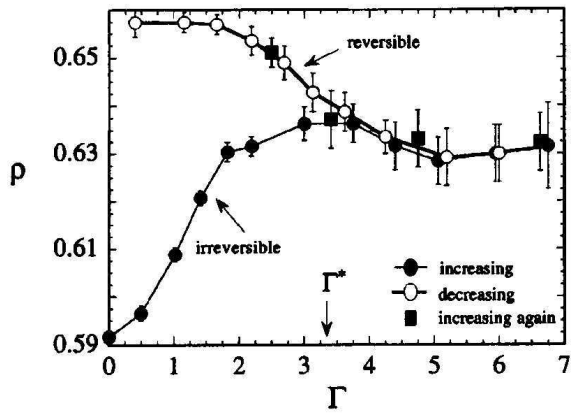
FIG. 2. The dependence of ρ on the vibration history. The beads were prepared in a low density initial configuration and then the acceleration amplitude Γ was slowly first increased (solid symbols) and then decreased (open symbols). At each value of Γ the system was tapped 10^5 times after which the density was recorded and Γ was subsequently incremented by $\Delta\Gamma \cong 0.5$. The upper branch that has the higher density is reversible to changes in Γ, see square symbols. The Γ^* denotes the irreversibility point.

Density fluctuations about the steady state

After the granular material has been vibrated for a sufficiently long time, it reaches a steady-state density ρ_{ss}. Although there is a well-defined average density, Fig. 1 already hints that there are large fluctuations about this value. The magnitude of the fluctuations depends on the vibration intensity and depth within the container. Figure 3 shows in more detail an example of these fluctuations as a function of time, $\delta\rho(t) = \rho(t) - \rho_{ss}$. In Fig. 3(a) we plot $\delta\rho(t)$ for a fixed value of acceleration, $\Gamma = 5.9$, but measured at different depths in the container. Note that the rate at which the density varies in time decreases with depth into the pile. That is, the top of the pile has more high frequency noise than the bottom. The curve marked "reference is the reference capacitor to which no vibrations are applied. This last curve is essential to compensate for drifts that could occur in the electronics over the very long period of our measurements. Each record shown here is 4096 taps long and up to 132 successive such records were assembled to produce one very long time sequence. Figure 3(b) shows the fluctuations in the density measured at the bottom capacitor as a function of acceleration Γ. As Γ is increased both the magnitude of the fluctuations and the amount of high-frequency noise increase.

From data as in Fig. 3 we can obtain the shape of the distribution function for the fluctuation amplitudes. We plot in Fig. 4 the logarithm of the relative probability of occurrence $D(\delta\rho)$ versus $\Psi^2 = (\rho - \rho_{ss})^2 \mathrm{sgn}(\rho - \rho_{ss})$

so that a Gaussian random process will have a triangular shape. In that figure we plot $D(\delta\rho)$ for the entire range of accelerations, $4 < \Gamma < 7$ for which fluctuations could be reliably measured with our equipment. All data records were corrected for instrumental drifts using the reference capacitor. As can be seen in Fig. 4, the majority of data shows Gaussian character. For a small fraction of runs e.g., ($\Gamma = 5.9$), however, we find significant deviations from Gaussian behavior, particularly near the middle and bottom of the pile. When such deviations are present they tend to preferentially occur for positive values of Ψ^2, i.e., higher densities. The deviations could be due to a metastable state, away from the mean, in which the system gets trapped. Fluctuations about this metastable state may even be distributed in a Gaussian fashion. The reason why such metastable states favor the lower portion of the column and why they are prominent at certain values of Γ is unclear.
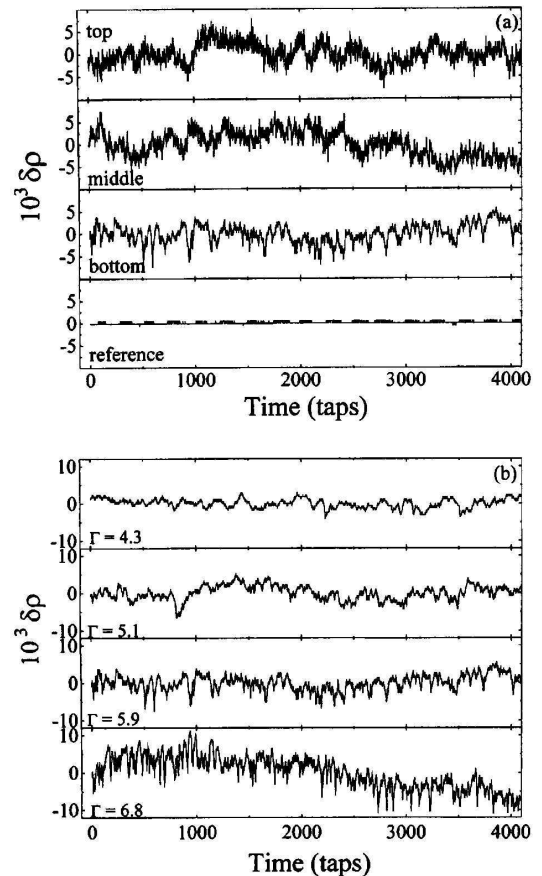
FIG. 3. Fluctuations in the volume density $\delta\rho(t) = \rho(t) - \rho_{ss}$ after the system has had sufficient time to relax to a steady-state density ρ_{ss}. In (a) the fluctuations at three different depths are shown for $\Gamma = 5.9$. The reference capacitor is used to correct for any instrumental drift. The dependence of the fluctuations on Γ is shown in (b) for the beads near the bottom of the pile. Fluctuations over a broad range of time scales are evident.

4

TOP   MIDDLE   BOTTOM

$\Gamma = 4.3$ $\Gamma = 4.3$ $\Gamma = 4.3$

$\Gamma = 5.1$ $\Gamma = 5.1$ $\Gamma = 5.1$

$\Gamma = 5.9$ $\Gamma = 5.9$ $\Gamma = 5.9$

$\Gamma = 6.8$ $\Gamma = 6.8$ $\Gamma = 6.8$

$D(\delta\rho)$

Ψ^2
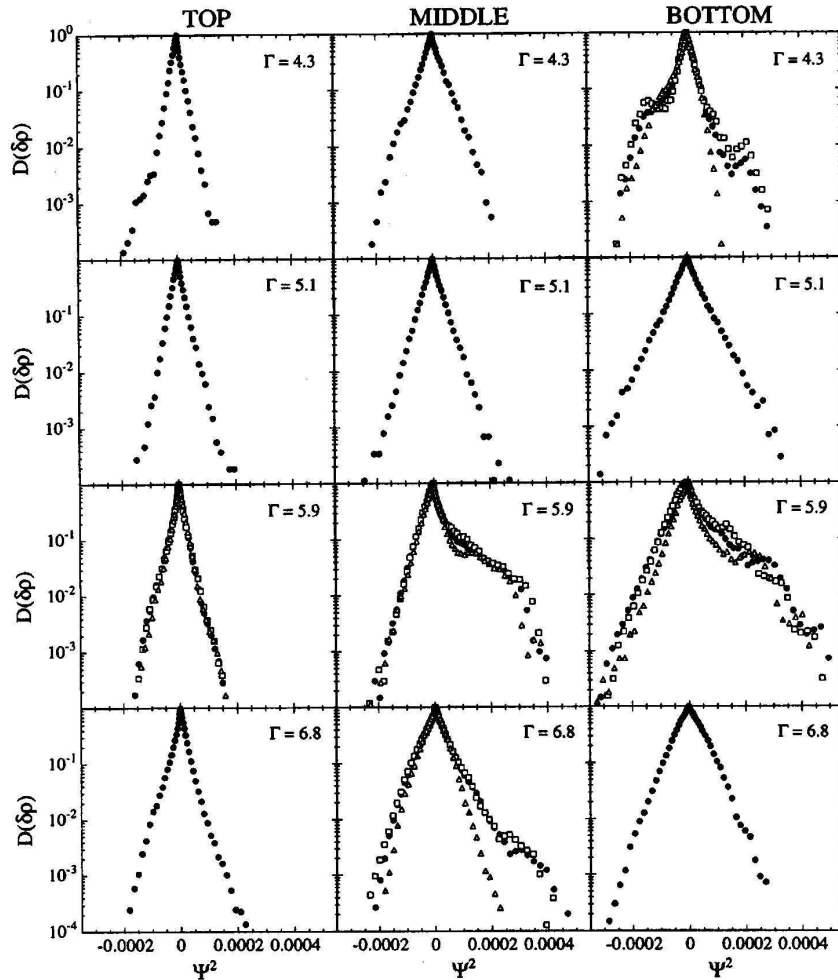
FIG. 4. The distribution functions $D(\delta\rho)$ for the occurrence of fluctuation amplitudes in the steady state are shown (solid circles) for the three depths at various G. Plotted as a function of $\Psi^2 = \delta\rho^2 \mathrm{sgn}(\delta\rho)$ a Gaussian distribution has a triangular shape. For selected panels, the time dependence of the distributions is shown by plotting the distribution functions for only the first (open squares) or second (open triangles) half of the time record. The majority of data appears stationary even when significant non Gaussian deviations are observed, e.g., at $\Gamma = 5.9$ near the middle and bottom of the pile.

We can qualitatively check whether the distribution functions correspond to a stationary random process or whether they conceal a slow drift away from an originally well-defined mean density. Strictly speaking, a stationary Gaussian process is one for which correlation functions of order higher than second are zero, see Ref. [18]). This is done by dividing each time record into two equal length halves and then determining the distribution functions for each half separately, as shown for selected values of Γ and depths by the open symbols in Fig. 4. We find that in practically all cases the fluctuations do appear to be stationary and, moreover, that in the very few nonstationary cases observed, the Gaussian character is recovered at *later* times (i.e., in the second half of the record).

By assembling 132 successive time traces of the type shown in Fig. 3, we can obtain continuous time records containing 540 672 data points. From such records we calculate both the density autocorrelation function and the power spectrum for the density fluctuations, $S_\rho(\omega)$, where the frequency v is measured in units of inverse taps. In Fig. 5 we plot $S_\rho(\omega)$ versus ω for the three depths at various values of acceleration, $\Gamma = 4.3$, 5.1, 5.9, and 6.8. We note several distinctive features to these power spectra. In particular, three characteristic regimes emerge: (i) a white noise regime, $S_\rho(\omega) \propto \omega^0$ below a low-frequency corner ω_L , (ii) an intermediate-frequency regime with nontrivial power-law behavior, and (iii) a simple roll-off $S_\rho(\omega) \propto \omega^{-2}$ above a high-frequency corner, ω_H. This classification appears to apply to all traces shown in Fig. 5. It is most pronounced for the spectrum in the lower right hand panel. For spectra where ω_L and ω_H are sufficiently separated in frequency, the data show that the spectral dependence between ω_L and ω_H cannot be approximated by just a simple superposition of two separate Lorentzians each having a frequency dependence $S \propto \tau/(1 + \omega^2\tau^2)$ but different characteristic times τ.

A comprehensive analysis of this region reveals that the most consistent description for all the data is obtained with a Lorentzian tail, $S_\rho(\omega) \sim \omega^{-2}$ just above ω_L , followed by a region with $S_\rho(\omega) \propto \omega^{-\delta}$ (with $\delta \approx 0.9 \pm 0.2$) stretching up to ω_H , the high-frequency corner.
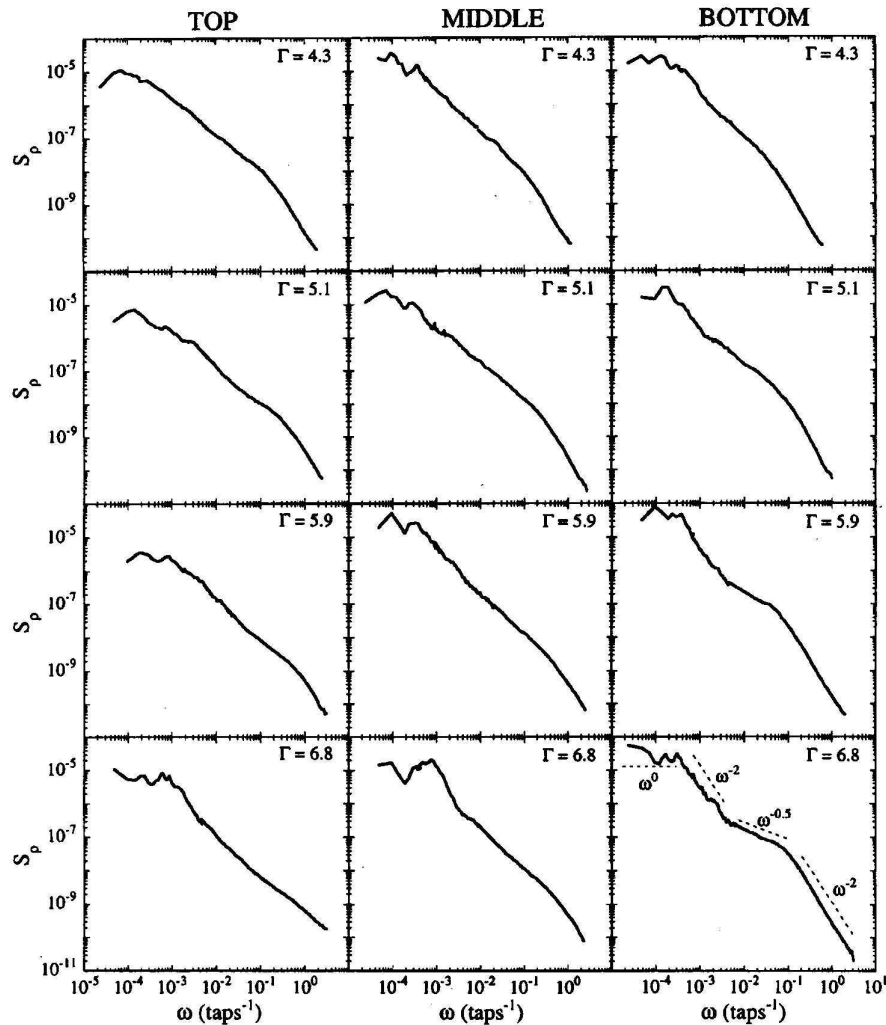
FIG. 5. The power spectral density S_ρ (taps) of the fluctuations as a function of frequency ω in the steady state is shown for the three depths at various Γ. For most spectra, two characteristic corner frequencies, ω_L and ω_H , are discernible which shift to higher frequencies for increasing Γ and decreasing depth. The characteristic regimes of behavior are denoted by the dashed lines in the lower right hand panel, which are guides to the eye.

One result from the data in Fig. 5 is the dependence of both corner frequencies on the acceleration Γ. To determine these frequencies we used a combination of two methods, which we illustrate here for the simple case of a Lorentzian spectrum. First, for any Lorentzian, the product ωS_ρ has a maximum precisely at $\omega = 1/\tau$ so that ω_L and ω_H can be associated with the frequencies at which ωS_ρ exhibits peaks. Second, even though we were using extremely long time records they are still of finite length. Figure 5 clearly indicates cases where ω_L is difficult to obtain because of the large statistical variance ($\approx 25\%$) in S_ρ throughout the lowest decade in frequencies. In these instances we employed the additional information contained in the one-sided sine transform of the density-density autocorrelation function. For example, for a single Lorentzian for which the autocorrelation function is simply $\approx e^{-t/\tau}$, the ratio of sine to cosine transform of the autocorrelation function is given by ωt, which depends only on t. A plot of this ratio versus v then allows one to obtain $\omega_L = 1/\tau$ even if this frequency falls *outside* the experimentally accessible frequency window. A detailed discussion of the more general case, where the signal consists of a superposition of independent fluctuators with a distribution of relaxation times τ will be presented elsewhere [19].
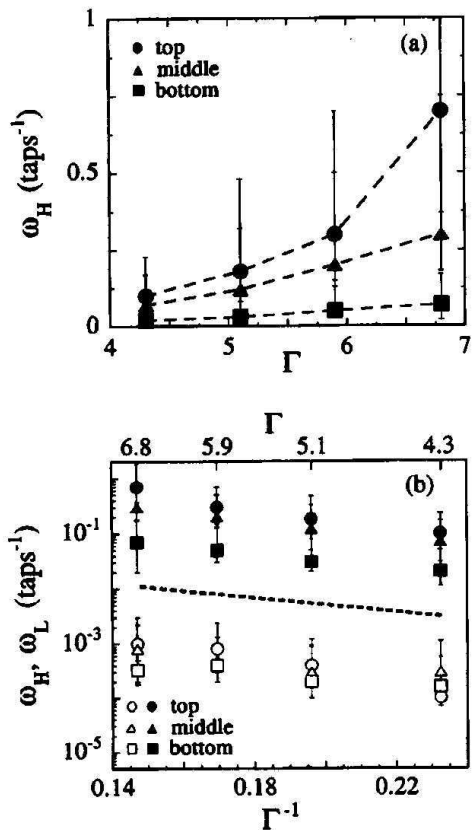
FIG. 6. The characteristic frequencies, ω_L (open symbols) and ω_H (solid symbols), in the power spectra plotted as a function of $1/\Gamma$. The general trend is for both ω_L and ω_H to increase with increasing Γ and decreasing depth into the pile. The dashed line in (b) is a guide to the eye, indicating that the trend is consistent with an activated-like behavior $\omega \approx \exp(-\Gamma_0/\Gamma)$, with Γ_0. For comparison, (a) shows the dependence of ω_H on Γ.

Figure 6 plots the resulting corner frequencies as a function of applied acceleration. The trend is for both ω_L and ω_H to increase as a function of increasing Γ and with decreasing depth into the pile, see Fig. 6(a). We note that over the relatively small available range of Γ, the variation of ω_H is consistent with behavior reminiscent of thermal activation: $\omega_H = \omega_0 \exp(-\Gamma_0/\Gamma)$. In this context, Γ_0 would represent an energy barrier and ω_0 would be an attempt frequency. We find that a value of $\Gamma_0 \approx 15$ is consistent with all the data, and that the greatest variation is in the parameter ω_0, which varies from 2×10^{-3} to 7×10^{-2} for ω_L and 1 to 15 for ω_H.

III. DISCUSSION

Several mechanisms [17,20-22] have been proposed to explain the kinetics of compaction. Although the proposed mechanisms are compelling, their quantitative predictions fail to describe the time dependence observed experimentally [1]. In light of our experimental results, we pay special attention to models based on free volume considerations as it appears that they not only capture the experimentally observed slow relaxation towards the steady state, but may also provide a valid framework for understanding the fluctuation spectrum. Such models [8-10,12,13] include strong nearest-neighbor repulsive interactions between particles that effectively block the occupation of adjacent sites. On very general grounds it is reasonable to assume that for the case of granular compaction, the rate of increase in volume density is exponentially reduced by free volume [23-25]. One alternative approach to the compaction problem is due to Linz [26] who proposes a phenomenological decay law for successive inverse packing fractions. Moreover, recent models based on the dynamics of crystalline clusters in the material have been proposed by Gavrilov [27] and by Head and Rogers [28]. These approaches lead to a time evolution that is essentially equivalent to Eq. (1).

A simple heuristic argument [12,24] for the compaction process illustrates how the effects of free volume can lead to the observed inverse logarithmic behavior. If each grain has a volume V_g and we start with a number n of grains per unit volume, then the volume fraction is given by $\rho = nV_g$. In general there exists a maximum possible volume fraction, $\rho_{\max}$, corresponding to the configuration of grains that occupies the least amount of volume. Then, at some volume fraction ρ, the average free volume available to each grain for rearrangements is $V_f = V_g(1/\rho - 1/\rho_{\max})$. During compaction, individual hardcore grains move, and when a void large enough to contain a grain is created, it is quickly filled by a new particle. When the volume fraction is large, voids the size of a particle are rare and a large number of voids must rearrange to accommodate an additional particle. We can estimate the rate of compaction by assuming that N grains must rearrange in such a way that they contribute their entire free volume to create a grain-sized void, $NV_f = V_g$. We find that this number increases as $N = \rho\rho_{\max}/(\rho_{\max} - \rho)$ during the compaction process. For independent, random grain motion during a tap, the probability for N grains to rearrange and open up a grain-size void is then e^{-N}. Consequently,

$$d\rho/dt \propto (1-\rho)e^{-\rho\rho_{\max}/(\rho_{\max}-\rho)}. \tag{2}$$

The rate at which the density increases is proportional to the void volume and the probability for such a rearrangement. The latter exponential factor reduces the rate and dominates for large ρ. In the limit $\rho \to \rho_{\max}$ we have $N \approx \rho_{\max}^2/(\rho_{\max} - \rho)$ and the solution of this equation is given asymptotically by $\rho(t) = \rho_{\max} - A/[B + \ln(t)]$, where A and B are constants [10,13,24,25]. This result closely approximates our experimentally based fitting form, Eq. (1), for the ensemble-averaged $\rho(t)$ as it approaches the steady state.

The solution to Eq. (2) always approaches the maximum density $\rho_{\max}$ and does not allow for a lower steady-state density. The reason that this model leads to jam-

ming is the absence of any void-creating mechanism that would be represented by a competing term on the right-hand side of Eq. (2). (The consequences of including a mechanism for the generation of voids are discussed in the next section for the "parking lot model and in Appendix A.) The competition between void annihilation and creation during tapping naturally leads to density fluctuations. We can also examine our data for the dependence of the corner frequencies on the acceleration Γ [Fig. 6(b)], where we found that $\omega_H = \omega_0 \exp(-\Gamma_0/\Gamma)$. We use the fact that ρ is a monotonic function of Γ in the reversible steady-state regime (Fig. 2) and write to first order $\rho(\Gamma) \approx \rho_{max} - m\Gamma$, where m is a positive constant, locally approximating the slope $\Delta\rho/\Delta\Gamma$ (see Ref. [14] for data on other bead sizes). Substituting in for Γ, the expression for ω_H can then be rewritten as $\omega_H = \omega_0 \exp[-m\Gamma_0/(\rho_{max} - \rho)]$. This has the same form as the right-hand side of Eq. (2) (in the limit that $\rho \rightarrow \rho_{max}$ and indicates that the kinetics depend sensitively on the available free volume, $1/\rho_{max} - 1/\rho$. As Γ is reduced and the density approaches the maximum density, the kinetics slow down rapidly. The manner in which the kinetics slow down is reminiscent of the Vogel-Fulcher form used to describe another class of disordered metastable materials, namely, glasses [29]. Similarities to glasses have recently been found in another approach to the compaction process [8-10].

IV. THEORETICAL MODEL AND SIMULATIONS OF COMPACTION

The parking lot model

In an attempt to explicitly work out some of the consequences of the free volume approach to granular compaction, we next discuss a simplified model. The model was previously studied in the context of chemisorption [23-25,30,31] and protein binding [32]. Despite its simple nature, it gives remarkably good qualitative agreement with the experimental data, both for the approach to the steady state and for the spectrum of fluctuations in the steady state. This model has the advantage that it readily lends itself to computer simulations; we restrict ourselves to the one-dimensional (1D) case, but extensions to higher dimensions are straightforward. Moreover, much is known about its low-density limit, for which mean-field equations exist that are amenable to analytic treatment (see the Appendix). In 1D, the model can be compared to parallel curbside parking where there are no marked parking spaces. For the person wishing to park a vehicle, the familiar situation is that there exist large, but not quite large enough, spaces between previously parked cars. The analogous question to the one we have been asking is "How many other cars have to be moved just a bit for the additional one to fit in?"
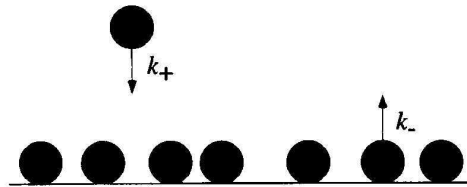
FIG. 7. The adsorption-desorption process. Adsorption is successful only in spaces large enough to accommodate a particle. Desorption of a particle, on the other hand, is unrestricted.

The model is defined as follows: identical particles of unit length adsorb uniformly from the bulk onto a substrate with rate k_+ and desorb with rate k_-. In other words, k_+ adsorption attempts are made per unit time per unit length, and similarly, the probability that an adsorbed particle desorbs in an infinitesimal time interval between t and $t + dt$ is k_-dt. While the desorption process is unrestricted, the adsorption process is subject to free volume constraints, i.e., particles cannot adsorb on top of previously adsorbed particles; see Fig. 7. This stochastic process is well-defined in arbitrary dimension and clearly satisfies detailed balance so that the system eventually reaches a steady-state density. In one dimension, $\rho_{max} = 1$.

Mapping the model on to the experiment, we associate an adsorption event with the annihilation or filling of a void within the pile of beads, whereas a desorption event is associated with the creation of a void. The ratio of adsorption to desorption rates, $k = k_+/k_-$, determines the final steady-state density in the model (see also the Appendix). Thus one can associate k in the model with the magnitude of the acceleration Γ in our experiment.

Simulation of compaction based on the parking lot model

In this section we compare the experimental results with Monte Carlo simulations of the 1D parking process. The details of the simulation are described elsewhere [24]. Here we report our results for a system size of 00 similar results were found for a system size of 25.

The simulations were started from a zero density initial state and allowed to evolve to various steady-state densities by varying k_- at a fixed value of $k_+ = 1$. In Fig. 8 we show the time evolution of the density as it approaches a steady-state density $\rho_{ss} = 0.84$. The steady-state densities obtained after equilibration coincide with those predicted by Eq. (A2a) in the Appendix. We find that the simulations reproduce the slow logarithmic relaxation towards the steady state in agreement with Eq. (1).
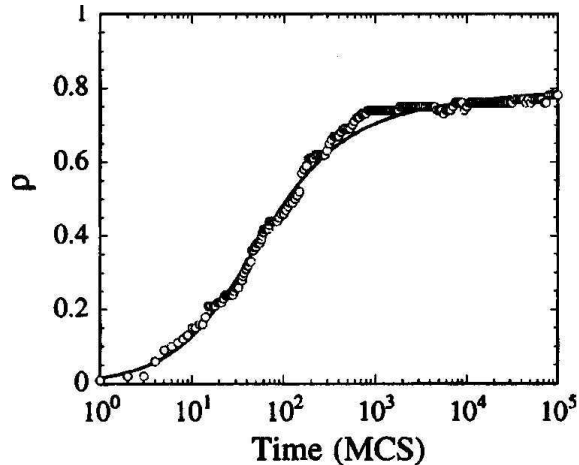
FIG. 8. The time evolution of the density in the simulation for $k = 10^3$ ($\rho_{ss} = 0.84$). Time is in units of Monte Carlo steps (MCS). The solid line represents a fit to Eq. (1).

FIG. 9. Power spectra, S_ρ (MCS), of the density fluctuations in the simulation of the one-dimensional parking process. The evolution of the spectral dependence is shown for values of the ratio $k = 33, 10^2, 10^3, 10^4$, corresponding to final steady-state densities $\rho_{ss} = 0.72, 0.77, 0.84$, and 0.88, respectively (see text). The strongest dependence on k is for ω_L, which decreases rapidly as the density increases. Such spectra are similar to those found in the experiment, see Fig. 5.

We now turn to the density fluctuations. In this case, the simulations ran long enough to ensure that a steady-state density was attained before density fluctuations were recorded. For low densities $\rho_{ss} < 0.37$ we find that in the simulation the power spectra of the fluctuations are best described by a Lorentzian having a single characteristic time scale, as expected from the mean-field analysis [see Eq. (A4) in the Appendix]. However, at higher densities (higher k) local fluctuations dominate the dynamics and the power spectra show the emergence of two distinct corner frequencies, which become progressively more separated. This is shown in Fig. 9 for a wide range of ratios k, where k_+ was fixed at a value of 1. Most notable is the low-frequency corner, which shifts rapidly to lower frequencies for small increments in density. By comparison, the high-frequency corner decreases much more slowly.

Our simulations find power spectra, $S_\rho(\omega)$, strikingly similar in shape to those obtained experimentally when $\rho_{ss} > 0.50$. Again we see three distinct regimes (Fig. 9). Below a corner frequency, ω_L, there is white noise $[S_\rho(\omega) \propto \omega_0]$. Above a high frequency corner, ω_H, $S_\rho(\omega) \propto \omega^{-2}$. The simulations offer the advantage of allowing the separation between ω_L and ω_H to be tuned by increasing the value of k or, equivalently, increasing the density. This allows the systematic investigation of the spectral dependence in the intermediate regime between the two corner frequencies. As in the experimental data, we find that there is a Lorentzian tail, $S_\rho(\omega) \propto \omega^{-2}$ just above ω_L. At higher frequencies, stretching up to the high-frequency corner ω_H, we find a power-law regime $S_\rho(\omega) \propto \omega^{-\delta}$. The exponent δ appears to depend slightly on the separation between the two corner frequencies. For the largest separations that span nearly 5 decades in frequency we find $\delta \approx 0.5$. This value is smaller than that found in the experimental data ($\delta \approx 0.9$), but again is inconsistent with a simple superposition of two Lorentzians having characteristic time scales ω_L^{-1} and ω_H^{-1}.

V. ANALOGY WITH THERMAL FLUCTUATIONS

In ordinary statistical mechanics, the fluctuation-dissipation theorem allows the determination of the response of a system to a small perturbation from its thermal fluctuations about equilibrium. In this section, we will explore the possibility that we can derive similar information about the granular system from its fluctuations about its steady-state density. In the granular thermodynamics theory developed by Edwards and coworkers, an analogy is made between granular and thermal systems. The basic assumption is that the *volume V* of a powder is analogous to the *energy* of a statistical system (we note that V here refers to the total volume and not just to the free volume). Instead of a Hamiltonian, there is a function that specifies the volume of the system in terms of the positions of the individual grains. The "entropy is thus the logarithm of the number of configurations: $S = \lambda \ln \int d$ (all configurations) where λ is the analog of Boltzmanns constant. Using this they defined a quantity analogous to a temperature in a thermal system, which they call the "compactivity X: $X = \partial V / \partial S$. In contrast to the notion of "granular temperature, which depends on the random motion of the particles, the compactivity characterizes the static system after it has reached a steady-state density via some preparation algorithm. Such an algorithm would be one as we have described above, where we have vibrated the granular system until it has reached the reversible steady-state density. If this theory is valid, then we should be able to define an

9

equilibrium such that two systems in equilibrium with a third system are also in equilibrium with each other. That is, no net volume will be transferred between the two systems when they are placed in contact with each other if they have the same value of X.

In a thermal system we can write the specific heat in two ways as follows:

$$C_V = dE_0/dT|_V = \langle (E - E_0)^2 \rangle / k_B T^2, \tag{3}$$

where E_0 is the equilibrium average of the energy E of the system, k_B is Boltzmanns constant, T is the temperature, and $\langle \cdots \rangle$ represents the time average. In Edwards theory for a powder the analogous quantity to the specific heat of a thermal system given in Eq. (3) becomes

$$C = dV_{ss}/dX = \langle (V - V_{ss})^2 \rangle / \lambda X^2, \tag{4}$$

where V_{ss} is the steady-state volume. Since we have measured the density fluctuations in the steady state (Figs. 3-5), we are in a position to explicitly calculate the variance, $\langle (V - V_{ss})^2 \rangle$, of volume fluctuations for a given steady-state volume V_{ss} defined here as $V_{ss} = 1/\rho_{ss}$. We can then write

$$\int_{V_1}^{V_2} dV_{ss}/\langle (V - V_{ss})^2 \rangle = \int_{X_1}^{X_2} dX/\lambda X^2 = 1/\lambda X_1 - 1/\lambda X_2. \tag{5}$$

Equation (5) allows us to measure the difference in compactivities for any two volumes as long as we know the fluctuations of the volumes (i.e., densities) as a function of the average volume. This is equivalent to obtaining the difference in temperatures for a thermal system between any two energies. Clearly, as V_{ss} increases X is expected to increase as well. Equation (5) allows the determination of an absolute value for the compactivity only once a suitable point of reference can be found. In Fig. 10 we show the experimentally obtained values of $\langle (V - V_{ss})^2 \rangle$ for several steady-state volumes along the reversible branch of Fig. 2 over the range $4 < \Gamma < 7$ [33]. The solid curve through the data for the top of the pile represents a linear fit to the function:

$$\langle (V - V_{ss})^2 \rangle = a + bV_{ss}, \tag{6}$$

where $a = -7.2 \times 10^{-4}$ and $b = 4.9 \times 10^{-4}$. This implies that the magnitude of the fluctuations goes to zero at $\rho = 0.68$, that is, near the close-packed density. Using this form for the dependence of the fluctuations on V_{ss} in Eq. (5) we find that

$$1/\lambda X \propto \ln(a + bV_{ss}). \tag{7}$$

This functional dependence is valid only over the limited range of experimental data, and may not be an adequate description of the general behavior. Below, we discuss a similar analysis for the simulation data for which a broader range of volumes can be explored. Using Eq.

(6), we can evaluate the difference in inverse compactivities between any two steady-state volumes. We find that $1/\lambda X_1 - 1/\lambda X_2 = 0.04$ where the subscripts 1 and 2 refer to the smallest and largest volumes for which we have data. This result explicitly demonstrates how the compactivity increases for larger volumes (smaller densities).

It is also interesting to consider the size of the fluctuating volumes that give rise to the observed variance. This can be estimated by assuming that the fractional fluctuations scale as $\langle \delta \rho^2 \rangle / \rho_{ss}^2 = \langle \delta V^2 \rangle / V_{ss} = \kappa^2 / N$, where $\delta V = V - V_{ss}$. This is the usual $N^{-1/2}$ classical self-averaging property of N in dependently fluctuating variables. The parameter κ accounts for the fact that there exists a maximum range of density changes for each grain that does not compromise the mechanical stability of the granular assembly. Figure 10 indicates that $\langle \delta V^2 \rangle / V_{ss}^2 > 1/40,000$, and as an upper bound we let $\kappa = \rho_{\text{xtal}} - \rho_{\text{RLP}} = 0.74 - 0.55 \approx 0.2$. We then find that $N > 1600$. Since we know that each capacitor averages over a volume corresponding to 6000 beads, this suggests that there are roughly 1600 independently fluctuating clusters each consisting of ~ 4 beads (lower bound).
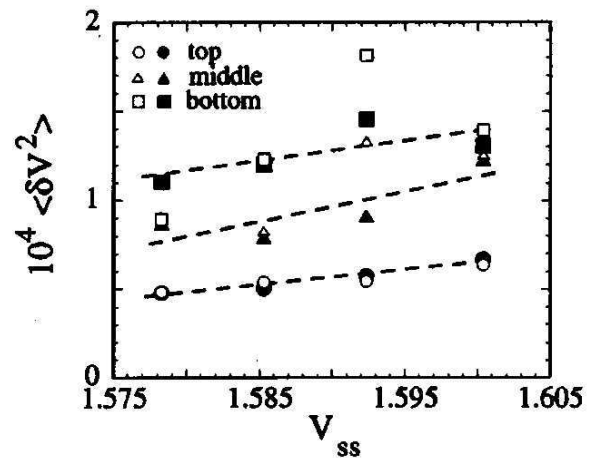
FIG. 10. The average variance of the experimental volume fluctuations (open symbols) as a function of the steady-state volume. The trend is for the variance to increase with increasing volume and *depth* into the pile. The solid symbols represent the variance as determined from the distribution of fluctuation amplitudes in Fig. 4 (see text). The dashed lines are linear fits to the solid symbols.

An important feature that can be seen in Fig. 10 is that the variance becomes systematically larger the deeper into the pile one goes [see also $D(\delta \rho)$ for $\Gamma = 5.1$ in Fig. 4]. For the middle and bottom sections of the column, the variance appears nonmonotonic with a peak near $V_{ss} = 1.592$, see open symbols in Fig. 10. Examination of the corresponding distributions of fluctuation amplitudes ($\Gamma = 5.9$ in Fig. 4) indicates that the increased

variance is due to a non-Gaussian tail in the distributions (see the description of Fig. 4, above). For comparison, we have also determined the variance from the slopes of the distribution functions in Fig. 4. We used the slopes corresponding to the low-density side of the distributions because these were most consistent with a Gaussian form over all accelerations and depths. In this way, the effect of the non-Gaussian tails in some of the distributions can be avoided. These results are shown as solid symbols in Fig. 10 and the dashed lines correspond to linear fits through the data. Here too, it is evident that the variance is larger for larger depths. A larger variance implies a correspondingly larger phase space. At first this seems counterintuitive be-cause the time records [Fig. 3(a)] and power spectra (Fig. 5) indicate that density fluctuations are slower at the bottom of the pile. Although the kinetics near the bottom of the pile may be slower, there is a greater number of configurations with different volumes that are accessible to those beads.
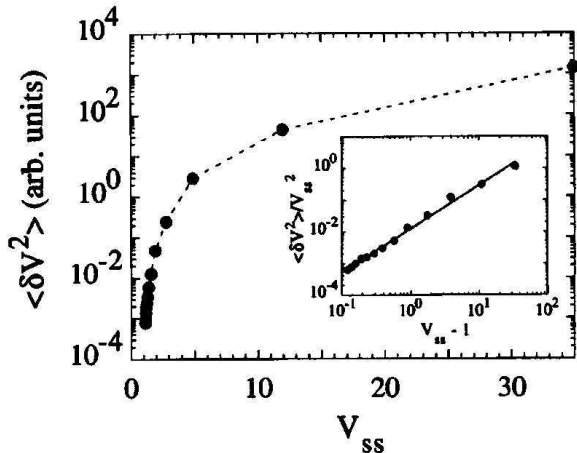
FIG. 11. The average variance of the volume fluctuations in the simulation as a function of the steady-state volume, V_{ss}. The fractional variance as a function of $V_{ss} - 1$ is plotted on logarithmic axes in the inset. The solid line is a power-law fit given by $0.0124(V_{ss} - 1)^{1.37}$.

A depth dependence to the variance also suggests the presence of a gradient in the compactivity. In Fig. 10, we used the average steady-state volumes V_{ss}, obtained from optical measurements of the total column height. One possibility is that this average volume density does not accurately represent the density in the different sections of the pile. If so, the larger compactivity near the bottom of the pile then implies that the bottom beads are actually in a less compact state than those at the top. However, from the trend in $\langle \delta V^2 \rangle$ versus V_{ss} in Fig. 10 the difference in packing fraction be-tween the top and bottom of the pile that would be necessary to have the variances be equal would be $\Delta\rho \approx 0.035$. Since this difference is huge on the scale of $\rho(\Gamma)$ for the reversible

branch in Fig. 2 we do not believe this to be a plausible explanation. Rather, it appears that there is another variable, such as pressure, in addition to the volume, that controls the depth dependence of the fluctuations. Indeed, supporting evidence to this effect can also be seen in Fig. 6, which shows that the high-frequency corner ω_H decreases with increasing depth into the pile. Nevertheless, we expect that the system is entirely jammed $\langle \delta V^2 \rangle \to 0$ at the same density (i.e., ρ_{max}) for all depths in the pile.
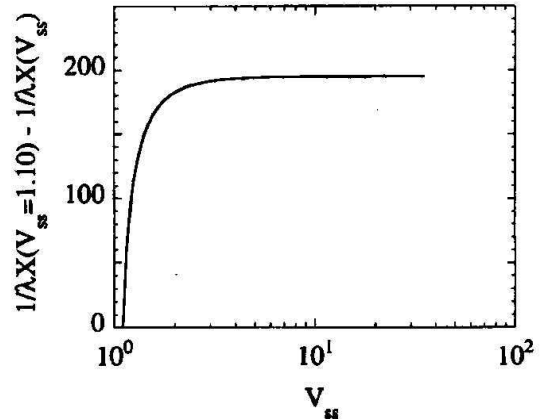
FIG. 12. The left hand side of Eq. (5) is numerically evaluated and plotted as a function of steady-state volume for the simulation data. As plotted, the difference in inverse compactivities between the highest density configuration ($V_{ss} - 1$) and a low density configuration (higher V_{ss}) can be read off directly.

With the simulation described above, a broader range of densities can be explored than that which is experimentally accessible. Figure 11 shows the dependence of the variance in volume fluctuations as a function of steady-state volume for the 1D parking lot model. The rapid decrease in variance near $V_{ss} - 1$ suggests that there may be a diverging length or time scale as the system approaches its most compact state. Indeed, plotting the normalized variance as a function of the free volume ($V_{ss} - 1$) does reveal power-law-like behavior $\langle \delta V^2 \rangle \propto (V_{ss} - 1)^\beta$ with $\beta \approx 1.4$. This is shown in the inset of Fig. 11. Proceeding with the compactivity analysis, the data in Fig. 11 was numerically integrated to yield the left-hand side of Eq. (5) to within a constant. An absolute value cannot be established with just our data. In Fig. 12 we plot the difference in inverse compactivity as a function of volume. This difference is with respect to the state $V_{ss} = 1.1$. Figure 12 indicates a nontrivial functional dependence to the increase in compactivity with system volume.

For comparison, the 3D experimental results correspond to relatively high densities in the 1D simulation because in 3D the available void volume is with respect to the random close packed limit (≈ 0.64) while the cor-

responding limit in 1D is 1. Taking this into account, the 30% increase in $\langle \delta V^2 \rangle$ in the experimental results shown in Fig. 10 compares well with the simulation data in Fig. 11 over a similarly restricted range in V_{ss}.

VI. CONCLUSIONS

In this paper, we have examined the volume fluctuations about a steady-state density for a granular system. For these measurements to provide a useful analogy with a thermal system, it is essential that the fluctuations be measured in steady-state conditions. For this reason, we have explicitly taken data on the reversible density line as shown in Fig. 2. From these measurements, we have been able to determine experimentally the compactivity, which is the quantity analogous to the temperature in the theory of Edwards et al.

Theories based on free volume seem particularly well suited for describing the data. As the system approaches its final state, a growing number of particles have to be rear-ranged in order for the density to be increased locally. The rate of increase in the density is exponentially reduced by this number leading to a logarithmically slow approach to the steady-state density as observed experimentally. Monte Carlo simulations of a one-dimensional adsorption-desorption process based on these ideas show fluctuations about the steady state density that are strikingly similar to those observed experimentally. These results attest to the importance of volume exclusion for granular relaxation and steady-state dynamics under vibration.

Despite this models simplicity and obvious shortcomings, it appears to capture an essential mechanism underlying the remarkably slow relaxation and the nature of the density fluctuations. This mechanism is associated with the reduction of free volume available for particle motion as the density increases. Although our simple model cannot predict the experimental values of the fitting parameters in Eq. (1), the inverse logarithmic density relaxation towards the steady state is the same one observed for granular compaction (see Fig. 1).

In the simulation model, our treatment was restricted to one-dimensional processes, but we expect that the results hold in higher dimensions as well. There are other important distinctions between the model and real granular media. One difference is that in the structure of a granular assembly the particles form contact networks. The creation of a void (a desorption event in the model) therefore requires the rearrangement of several particles and is thus restricted just as is the annihilation of voids. Another difference is the mechanical stability of a granular assembly. This property will place limits on the free volume available for large void creation. For instance, for spherical particles in three dimensions and in the presence of gravity the available free volume is deter-mined by the restricted range of accessible volume fractions,

namely, between the random close packed $\rho \approx 0.64$ and random loose packed $\rho \cong 0.55$ configurations.

It is interesting to speculate whether the reduction in free volume leads to a crossover from a simple independent particle picture for compaction to a more complex process at higher densities, presumably involving correlations over increasingly longer length and time scales. In this regard, we have demonstrated that density fluctuations are an important probe of the underlying microscopic dynamics. Indeed, the study of fluctuations may elucidate the physics of independent and cooperative-particle motions, which lead to the macroscopic response of a powder subject to vertical vibrations. For instance, it is interesting to note that from both the experimental and simulation data there appear to be two characteristic time scales, related to the corner frequencies ω_L and ω_H in the power spectra, that characterize the steady-state dynamics. This behavior may be related to the results found in 3D simulations of vibrated powders by Mehta and Barker [17,20,34] and in simulations of a frustrated lattice gas [8-10]. Those results suggested the existence of two exponential relaxation mechanisms: the faster of the two involves the motions of independent particles while the slower involves collective particle motions, which were found to be diffusive. However, we emphasize again that both our experimental and simulation data are not consistent with a superposition of two independent exponentially decaying processes.

In this paper we have presented results for monodisperse spherical particles subject to vertical shaking. Realistic powders are far more complicated with properties that depend on factors like cohesive forces, polydispersity in size, and ir-regularity or anisotropy in shape. Nevertheless, our results can provide a valuable benchmark for evaluating the predictions of theoretical models and simulations. The applicability of concepts such as compactivity or "granular temperature in the description of quasistatic granular media requires further exploration. In particular, it would be interesting to ex-amine the properties of granular systems comprised of particles with shape anisotropies and subject to isotropic shaking. Furthermore, our experimental data suggest that the steady-state properties of a granular assembly cannot be fully described by a single state variable, i.e., the volume. Rather, another variable is required to account for the depth dependence of the volume fluctuations.

Note added in proof. The width of the density fluctuations in the parking lot model can be calculated in the mean-field approach described in the Appendix. For details see E. Ben-Naim et al., Physica D (to be published). Such calculation predicts a power law as seen in the inset to Fig. 11 for the simulation data, but with an exponent $\beta = 2$.

VII. ACKNOWLEDGMENTS

APPENDIX

For the one-dimensional parking lot model an analytical mean-field description exists. On the continuum, an approximate rate equation for the density evolution was constructed from the exact steady-state void distribution. This equation yields an approach to the steady state that is essentially identical to that found in the experiment [i.e., Eq. (1)]. However, it is less successful in capturing the fluctuation behavior, particularly for the high densities relevant here. We summarize the salient analytic results for the model. Details can be found in Refs. [23-25]. A modified Langmuir equation can be written for the rate of change in density [24]:

$$d\rho/dt = k_+(1 - \rho)e^{-\rho/(1-\rho)} - k_-\rho. \quad (A1)$$

The gain term is proportional to the fraction of unoccupied space, which is modified by an "excluded volume constraint. It was previously shown that in steady state the prob-ability $s(\rho)$ that an adsorption event is successful is given by $s(\rho) = e^{-\rho/(1-\rho)}$ [24]. This so-called "sticking coefficient vanishes exponentially as $\rho \to 1$. This effectively reduces the sticking rate, $k_+ \to k_+(\rho) = k_+ s(\rho)$. The desorption process, on the other hand, is unrestricted and so the loss term is proportional to the density itself. The steady-state density ρ_{ss}, which is obtained by imposing $d\rho/dt = 0$, can be determined as a function of the adsorption to desorption rate ratio, $k = k_+/k_-$, from the following transcendental equation:

$$\alpha e^{\alpha} = k, \qquad \text{with} \qquad \alpha = \rho_{ss}/(1 - \rho_{ss}). \quad (A2a)$$

The following leading behavior in the two limiting cases is found

$$\rho_{ss}(k) \cong \begin{cases} k, & k \ll 1; \\ 1 - (\ln k)^{-1}, & k \gg 1. \end{cases} \quad (A2b)$$

The effect of the volume exclusion constraint is striking, a huge adsorption to desorption rate ratio, $k > 10^9$, is necessary to achieve a 0.95 steady-state density. We now focus on the relaxation properties of the system. The granular compaction process corresponds to the high density limit, and we thus consider the desorption-controlled case, $k \gg 1$. Hence, let us fix $k_+ = 1$ and consider the limit $k_- \to 0$ of Eq. (A1). For $t \gg 1/k_+$, it can be shown that the system approaches complete coverage, $\rho_\infty = 1$, according to [24,25]

$$\rho(t) \cong \rho_\infty - 1/(\ln k_+ t). \quad (A2)$$

This is confirmed by numerical simulations in one dimension (see Ref. [24] and Sec. IV). We conclude that the excluded volume constraint gives rise to a slow relaxation.

Equation (A3) holds indefinitely only for the truly irreversible limit of the parking process, i.e., for $k = \infty$. For large but finite rate ratios, the final density is given by Eq. (A2b). By computing how a small perturbation from the steady state decays with time, an exponential relaxation towards the steady state is found $|\rho_{ss} - \rho(t)| \propto e^{-1/T}$ for $t \gg 1/k_-$. The relaxation time is

$$T = (1 - \rho_{ss})^2/k_-. \quad (A3)$$

The above results can be simply understood: the early time behavior of the system follows the irreversible limit of $k_- = 0$. Once the system is sufficiently close to the steady state, the density relaxes exponentially to its final value.

[1] J. B. Knight et al., Phys. Rev. E **51**, 3957 (1995).
[2] S. F. Edwards and R. B. S. Oakeshott, Physica A **157**, 1080 (1989).
[3] A. Mehta and S. F. Edwards, Physica A **157**, 1091 (1989).
[4] S. F. Edwards and C. C. Mounfield, Physica A **210**, 290 (1994).
[5] S. Ogawa, in Proceedings of the U.S.-Japan Symposium on Continuum Mechanics and Statistical Approaches in the Me-chanics of Granular Materials, edited by S. C. Cowin and M. Satake (Gakujutsu Bunken Fukyukai, Tokyo, 1979).
[6] C. S. Campbell, Annu. Rev. Fluid Mech. **22**,57 (1990).
[7] I. Ippolito et al., Phys. Rev. E **52**, 2072 (1995).
[8] A. Coniglio and H. J. Herrmann, Physica A **225**, 1 (1996).
[9] M. Nicodemi, A. Coniglio, and H. J. Herrmann, J. Phys. A **30**, L379 (1997).
[10] M. Nicodemi, A. Coniglio, and H. J. Herrmann, Phys. Rev. E **55**, 3962 (1997).
[11] H. M. Jaeger, S. R. Nagel, and R. P. Behringer, Phys. Today **49**, 32 (1996).
[12] H. M. Jaeger, S. R. Nagel, and R. P. Behringer, Rev. Mod. Phys. **68**, 1259 (1996).
[13] P. G. de Gennes (unpublished);
[14] T. Boutreux and P. G. de Gennes, Physica A **224**,59 (1997).
[15] E. R. Nowak et al., Powder Technol. **94**, 79 (1997).
[16] J. B. Knight, H. M. Jaeger, and S. R. Nagel, Phys. Rev. Lett. **70**, 3728 (1993).

[17] K. Shinohara, in Handbook of Powder Science and Technology, edited by M. E. Fayed and L. Otten (van Nostrand Rein-hold Co., New York, 1984).

[18] A. Mehta and G. C. Barker, Phys. Rev. Lett. **67**, 394 (1991).

[19] M. Nelkin and A.-M. S. Tremblay, J. Stat. Phys. **25**, 253 (1981).

[20] E. R. Nowak, S. R. Nagel, and H. M. Jaeger (unpublished).

[21] G. C. Barker and A. Mehta, Phys. Rev. E **47**, 184 (1993).

[22] H. S. Caram and D. C. Hong, Phys. Rev. Lett. **67**, 828 (1991).

[23] D. C. Hong et al., Phys. Rev. E **50**, 4123 (1994).

[24] G. Tarjus and P. Viot, Phys. Rev. Lett. **68**, 2354 (1992).

[25] P. L. Krapivsky and E. Ben-Naim, J. Chem. Phys. **100**, 6778 (1994).

[26] X. Jin, G. Tarjus, and J. Talbot, J. Phys. A 27, L195 (1994).

[27] S. J. Linz, Phys. Rev. E **54**, 2925 (1996).

[28] K. Gavrilov (unpublished).

[29] D. A. Head and G. J. Rodgers (unpublished).

[30] M. D. Ediger, C. A. Angell, and S. R. Nagel, J. Phys. Chem. **100**, 13200 (1996).

[31] V. Privman and M. Barma, J. Chem. Phys. **97**, 6714 (1992).

[32] J. W. Evans, Rev. Mod. Phys. **65**, 1281 (1993).

[33] J. D. McGhee and P. H. von Hippel, J. Mol. Biol. **86**, 469 (1974).

[34] The variance is also equal to the integrated power spectrum over all frequencies. Because the power spectral dependence is weaker than ω^{-2} at lowest frequencies and tends to fall off as ω^{-1} at the highest frequencies we can have confidence that the variance is finite.

[35] G. C. Barker and A. Mehta, Phys. Rev. A **45**, 3435 (1992).